Noise-optimized ultrastable low-noise current amplifier EP

C. Krause ⓘD, D. Drung ⓘD, M. Götz ⓘD, and H. Scherer ⓘD

COLLECTIONS

EP   This paper was selected as an Editor's Pick

View Online   Export Citation   CrossMark

ARTICLES YOU MAY BE INTERESTED IN

Noise-optimized ultrastable low-noise current amplifier (EP)

View Online   Export Citation   CrossMark

C. Krause,[1,a] (iD) D. Drung,[1,b] (iD) M. Götz,[2] (iD) and H. Scherer[2] (iD)

AFFILIATIONS

[1] Physikalisch-Technische Bundesanstalt (PTB), Abbestraße 2-12, 10587 Berlin, Germany
[2] Physikalisch-Technische Bundesanstalt (PTB), Bundesallee 100, 38116 Braunschweig, Germany

[a] **Electronic mail:** Christian.Krause@ptb.de
[b] **Electronic mail:** Dietmar.Drung@ptb.de

ABSTRACT

We have developed a noise-optimized ultrastable low-noise current amplifier (ULCA) aimed at reducing the uncertainty at low currents. It involves a thin-film resistor network with 6.75 GΩ at the high-ohmic path which reduces the noise level to $1.6 \, \mathrm{fA}/\sqrt{\mathrm{Hz}}$. Noise investigations as well as short-term and long-term stability studies were carried out. The stability of the input current gain was measured using a cryogenic current comparator at ±6.1 nA. Methods for investigating the measurement accuracy at low input currents of about 100 pA at a level of below one part in 10^7 are introduced and experimentally verified. The performance of the noise-optimized ULCA is compared with that of the standard variant introduced in 2014. It is shown that the reduced noise floor is achieved without impairing the stability of the transresistance.

I. INTRODUCTION

In various fields of research and also industry, for example in dosimetry, the interest in the metrology of electric currents in the femtoampere to nanoampere range is increasing.[1] Therefore, pushing the sensitivity and accuracy limits of related small-current instrumentation (meters and sources) is highly relevant. Regarding instrument calibrations in general, the demands on the calibration uncertainties and intervals depend on the accuracy required for the particular application. The ultimate challenge is found in the research field of single-electron pumps (SEPs). Typically, SEP-generated currents are of the order of 100 pA, and uncertainties of 0.1 parts per million (ppm) or below are demanded.[2,3] Until 2014, achieving such a low current measurement uncertainty was not possible, neither with commercial equipment nor with special metrological setups.[4,5] This lack gave rise to a new type of small-current meter, the ultrastable low-noise current amplifier (ULCA).[6,7] This instrument not only enables the highest current measurement performance, but also is very versatile and allows the generation of small currents with

high accuracy. Thanks to its excellent measurement accuracy, the ULCA provides sufficient stability for performing a future quantum metrological triangle experiment with SEP.[8]

In the past years, the ULCA demonstrated its performance in several low-current applications. For example, it enabled the measurement of SEP generated currents of about 100 pA with uncertainties down to 0.16 μA/A[9] (all uncertainties quoted in this paper are standard uncertainties, with coverage factor $k = 1$). In 2015, it was used as a travelling standard confirming sub-ppm consistency in the current measurement capabilities of three National Metrology Institutes (NMIs).[10] Recently, an inter-laboratory comparison between NPL and PTB was conducted, in which consistency at the level of 0.2 μΩ/Ω was reached, thanks to improved calibration capabilities at NPL.[11] Furthermore, a study was presented in which several commercial picoammeters were calibrated with the ULCA as a calibrator current source in the range of 1 fA–1 μA, again confirming the ULCAs superior performance.[12]

Generally, for measurements limited in uncertainty by the presence of white noise, the statistical (Type A) uncertainty is

proportional to the rms noise level divided by the square root of the measurement time. Hence, a reduction of the rms noise by a factor x reduces the measurement time that is required to achieve the same uncertainty by a factor of x^2. Therefore, the development of an ULCA tailored for improved measurement uncertainty at low currents (100 pA and less) was based on the maximum reduction of the instrument's noise level achieved without impairing the stability of the gain factor (transresistance). The noise optimization of the new ULCA and a comparison with previous variants[6,13] are discussed in Sec. II. Stability measurements (short-term as well as long-term) obtained with a cryogenic current comparator (CCC) are shown in Sec. III. Methods for evaluating the accuracy at small currents are presented in Sec. IV, together with measurement results obtained with the new ULCA. A short conclusion is given in Sec. V.

II. NOISE OPTIMIZATION

To obtain the highest levels of accuracy, ULCA instruments are designed as a two-stage amplifier (current-to-voltage converter).[6] The first stage provides a current amplification by a factor of G_I and the second stage provides a current-to-voltage-conversion via a resistance R_{IV}. Both stages are individually calibrated, typically using CCC setups.[6,11] The total transresistance A_{TR} of the ULCA is given by the product of G_I and R_{IV}.

The current amplification in the first stage is realized by using a resistor network. This network consists of several thousand individual chip resistors forming a high-ohmic and a low-ohmic path with the resistance ratio of G_I. As described in Ref. 13, the amplifier noise is dominated by thermal noise in the resistance R of the high-ohmic path of the network. For the standard variant of the ULCA in Ref. 6, $R = 3$ GΩ, is formed by a series connection of 2 MΩ thin-film chip resistors (0805 size = 2 mm × 1.25 mm[14]). This results in a noise floor of 2.4 fA/$\sqrt{\text{Hz}}$, including a small contribution of the input amplifier.

To further reduce the noise level, a higher resistance R is necessary. This can be achieved by increasing the resistance of the chip resistors and/or connecting more resistors in series. Obviously, chip resistors with higher resistance values are easier to implement rather than enabling an increase in number, as this requires a redesign of the network. However, at the time of development, 2 MΩ was the highest available value for resistors in thin-film technology and in 0805 package size. Higher resistance values in this size were only available in thick-film technology, but are not useable here for reasons of stability. Therefore, we redesigned the resistor board to increase the number of resistors from about 3000 to 4000. The additional 1000 resistors were placed on the high ohmic path to get a series-connection of 2500 resistors. With 2 MΩ per resistor, this results in a total resistance $R = 5$ GΩ. Additionally, after the redesign of the network board, new high-ohmic 2.7 MΩ thin-film chip resistors became available on the market. Both improvements result in a resistance network with $R = 6.75$ GΩ and a corresponding amplifier noise floor

of 1.6 fA/$\sqrt{\text{Hz}}$. The current gain ($G_I = 1000$) and the output transresistance ($R_{IV} = 1$ MΩ) remain unchanged.

Figure 1 shows the noise comparison of the standard ULCA[10] with $R = 3$ GΩ (units U0006 and U0007) as well as the new noise-optimized variant with $R = 6.75$ GΩ (units U0020 and U0033). Each measurement was performed with a cover cap mounted at the input to avoid electromagnetic pickup. In panel (a) the spectral densities are depicted from 0.1 mHz to 5 Hz. Panel (b) shows the corresponding Allan deviation plots for sampling times τ between 10 s and 10^5 s. Fit approximations for white noise and $1/f$ noise are shown by red dashed lines. They are determined according to the data analysis described in Sec. III of Ref. 13. As expected, the white noise level of the noise-optimized variant is a factor of $\sqrt{6.75\,\text{GΩ} / 3\,\text{GΩ}} = 1.5$ lower than the standard variant. In practice, this reduces the measurement time at low currents by up to a factor of 2. Note that the standard and noise-optimized variants have nearly equal $1/f$ corner frequencies. As will be shown later, regardless of the noise level, both ULCA variants exhibit the same stability and accuracy level.

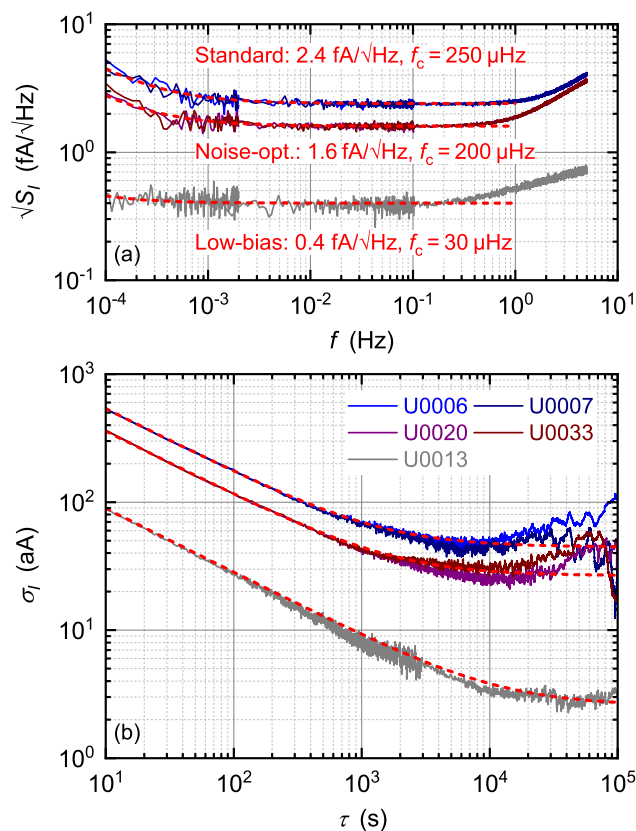**FIG. 1**. Noise comparison of three ULCA variants: standard (U0006 and U0007), noise-optimized (U0020 and U0033), and low-bias (U0013). (a) Spectral density, (b) Allan deviation. U0013 shows the lowest noise floor thanks to a thick-film resistor network with $R = 185$ GΩ, but its stability is about a factor of 100 worse compared to the other two variants. Red dashed lines show approximations for white and $1/f$ noise.

The lowest ULCA noise level achieved so far was obtained with the low-bias variant being equipped with a thick-film resistor network of R = 185 GΩ.[13] For comparison, the noise level of a low-bias unit (U0013) is also depicted in Fig. 1. It reaches 0.4 fA/$\sqrt{Hz}$ with an extremely low $1/f$ corner of about 30 μHz. However, in terms of accuracy and stability, it is about two orders of magnitude worse than the other two variants due to the thick-film technology used for the resistor network. Therefore, this variant will not be discussed in the remainder of this article.

III. CCC-BASED STABILITY EVALUATION

To minimize the calibration uncertainty, the input and output stages of an ULCA are separately calibrated with a CCC.[6] At PTB, the 14-bit CCC[15] is routinely used which is equipped with 14 windings having numbers of turns ranging from 2^0 to 2^{13}. Together with 5 additional windings, in total 18 276 turns are accessible at the room temperature interface.[16] For the input stage calibration, relatively large calibration currents are applied to improve the signal to noise ratio. The limit is set by the input stage voltage range of ±44 V divided by the resistance R. Hence, the input stage of the noise-optimized variant is calibrated with a lower current (±6.1 nA instead of ±13 nA according to the resistance ratio 3 GΩ/6.75 GΩ). This increases the calibration uncertainty of G_I from 0.01 μA/A to 0.02 μA/A. The calibration uncertainty of the output stage is 0.01 μΩ/Ω for both variants, since the output stages are of identical design and the same calibration current of ±0.5 μA is used.

The "±" indicates periodic reversal of the current during calibration. This is common practice for precise dc measurements to suppress low-frequency noise and offset. For the analysis of the corresponding measurement data in this paper, the full signal amplitude (i.e., the difference between the output levels at both current polarities) is considered. To determine the amplitude from the raw data, a standard algorithm is used which calculates a measurement point out of three signal "plateaus," corresponding to the adjacent −/+/− sequences of the data. A detailed description can be found in the supplementary of Ref. 17. For instance, the second half of the first plateau, the complete second plateau, and the first half of the third plateau (and repeated for the whole sequence of data) can be used for this kind of analysis. To suppress settling effects, the corresponding transient data after each current reversal are removed.

Using the 14-bit CCC and the above described analysis method, short-term stability observations were carried out, i.e., gain fluctuations were measured over a period of about two weeks. In terms of stability, the input stage (G_I) is more critical than the output stage due to the high resistance R and the correspondingly low current levels (the current level at the output stage is a factor of 1000 larger and hence a resistor technology yielding superior stability is applied). Therefore, the input stages of two ULCA variants were investigated: the standard variant U0005 with R = 3 GΩ and the noise-optimized variant U0033 containing the new resistor network with

R = 6.75 GΩ. The 14-bit CCC can be operated in the battery-powered mode for up to about a day. This is more than sufficient for the ULCA calibration, which has a duration of 100 min, but not enough to make a statement about short-term fluctuations. Consequently, mains operation was used for the stability measurement depicted in Fig. 2. The measurement period was about two weeks for both ULCAs. Each data point was taken over an integration time of τ = 6000 s which equals the duration of a regular calibration. The level of the fluctuations is in the order of one part in 10^7. As expected from the difference in the measurement currents, U0033 shows larger fluctuations than U0005.

The relative changes $\Delta G_I/G_I$ in Fig. 2 refer to a regular calibration (i.e., with the battery mode) performed prior to the measurement. It was observed that activating the charging shifted the value of $\Delta G_I/G_I$ by about −50 nA/A or −100 nA/A for U0005 or U0033, respectively. This is presumably caused by electromagnetic interference produced by the battery chargers leading to noise rectification in the superconducting quantum interference device (SQUID).[16] The uncertainty budget of the calibration assumes a uniformly distributed error flux of ±0.5 $\mu\Phi_0$, where Φ_0 is the flux quantum.[18] This value was deduced from the nonlinearity measurements in Ref. 16 and implies an error current within about ±350 aA for the 16 000 turns of the CCC winding connected to the ULCA input. The shift of $\Delta G_I/G_I$ in Fig. 2 due to battery charging corresponds to an error flux of about ±2 $\mu\Phi_0$.

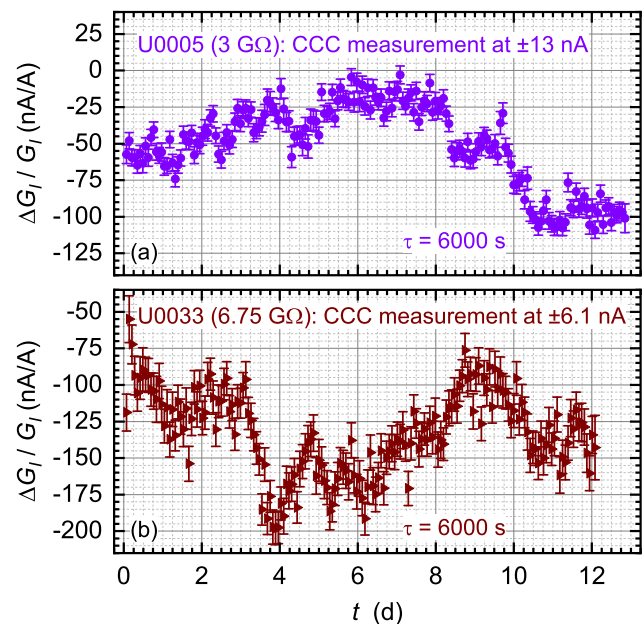**FIG. 2**. Stability measurement of G_I for two ULCA variants using the 14-bit CCC: (a) standard variant U0005 (R = 3 GΩ) and (b) noise-optimized variant U0033 (R = 6.75 GΩ). The relative changes $\Delta G_I/G_I$ refer to a regular calibration before measurement. Due to the long measuring period, the CCC was used in mains operation and not in the battery mode as during a calibration.
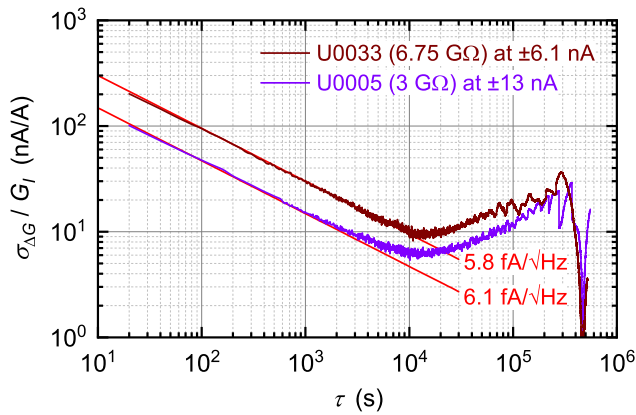
FIG. 3. Allan deviation of the stability measurement performed with 14-bit CCC for U0005 and U0033. The red lines show the noise level for both ULCAs including CCC.

It is yet unclear whether the stronger noise rectification also deteriorates the stability investigation. Therefore, the intrinsic ULCA stability might even be better than depicted in Fig. 2.

Figure 3 illustrates the Allan deviation of the data from the stability measurement in Fig. 2. Due to the smaller calibration current, the relative uncertainty found for U0033 is higher than that for U0005. The red lines represent the corresponding white noise level according to Eq. (2) in Ref. 6. Note that this level indicates that the noise is dominated by the CCC. By subtracting the ULCA noise contribution, a noise floor of $5.6 \text{ fA}/\sqrt{\text{Hz}}$ is found for the CCC. This is close to the typical value of $5 \text{ fA}/\sqrt{\text{Hz}}$ quoted in Ref. 19.

Since the first ULCA prototypes were put into operation in 2014, a large number of calibrations have been performed on various ULCA units. Based on these calibration measurements, Fig. 4 is obtained. It shows results for seven ULCA units within a period of about four years and allows a conclusion to be drawn on long-term stability behavior. Each data point represents a calibration that was performed with a 12-bit or a 14-bit CCC.[15,20] In addition, for each data point, the corresponding ULCA initial calibration result was subtracted to allow a fine-scale comparison of long-term stability in one diagram. Five of the seven depicted ULCAs are standard variants with $R = 3 \text{ G}\Omega$ put into operation between 2014 and 2015. The calibration series of the two noise-optimized prototypes U0020 and U0033 ($R = 6.75 \text{ G}\Omega$) started in late 2017. The relative deviation in terms of initial calibration is shown in (a) for the input current gain $\Delta G_I/G_I$, in (b) for the output transresistance $\Delta R_{IV}/R_{IV}$, and for the total transresistance $\Delta A_{TR}/A_{TR}$ in (c).

The drift in the input current gain of the ULCA units in Fig. 4(a) is typically within $\pm 1 \, \mu\text{A/A}$ per year, indicated by a gray meshed area. However, U0003 shows a large change in 2017. We attribute this behavior to the fact that the resistor network in this unit was the very first prototype of the final design, with components that were placed and soldered by
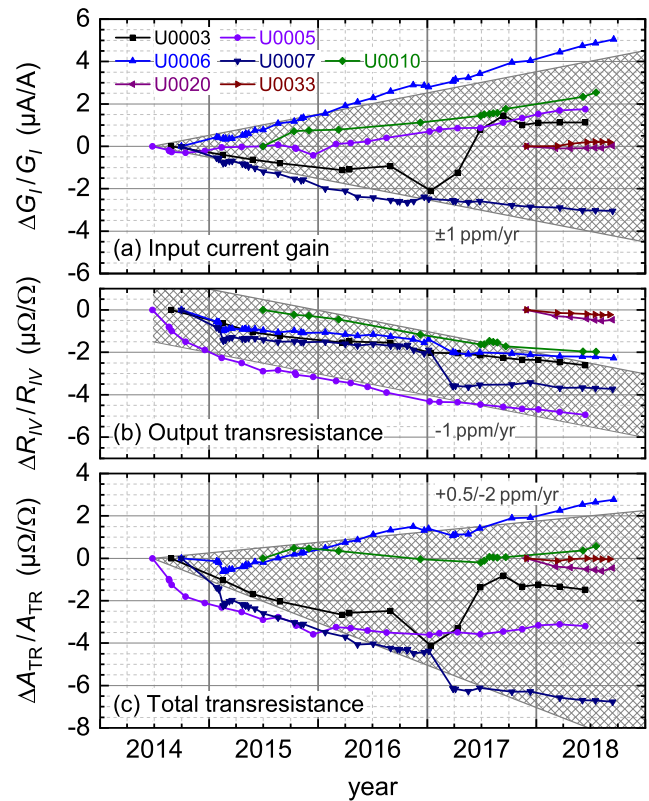

FIG. 4. Long-term stability of (a) input current gain, (b) output transresistance, and (c) total transresistance in terms of relative deviation from the initial calibration over five years. With the exception of the noise-optimized variants U0020 and U0033, all ULCAs are standard variants.

hand (all other networks were assembled using a pick-and-place machine and a reflow oven). Hand-soldering compared to an automated assembly combined with a reflow oven is less uniform and, thus, causes more thermal stress of the individual resistors and therefore larger parameter scatter. Strong differences in the relaxation processes of each individual resistor and their respective aging behavior are supposed to degrade the current gain stability. This might explain the worse long-term stability of this input stage compared to all other units.

In Fig. 4(b) the gray meshed area covering the data points indicates a typical negative drift of about $-1 \, \mu\Omega/\Omega$ per year for $\Delta R_{IV}/R_{IV}$ (except for a few discontinuities which will be discussed later). For all units, $R_{IV} = 1 \text{ M}\Omega$ is realized by a set of 14 Vishay VHP101 foil resistors connected in series. According to the data sheet, the shelf life stability is typically $\pm 2 \, \mu\Omega/\Omega$ after 6 years, which implies a mean annual drift of up to $\pm 0.33 \, \mu\Omega/\Omega$.[21] The reason for the discrepancy is yet not understood.

Figure 4(c) shows the variation of A_{TR} calculated from the results of the data for G_I and R_{IV}. As the annual drift of G_I scatters between about $\pm 1 \, \mu\text{A/A}$ and the drift of R_{IV} is negative, the

TABLE I. Change of G_I, R_{IV}, and A_{TR} after international transport to various NMIs worldwide. The abbreviations DE, UK, FR, FI, CH, KR, and TR refer to the countries and the corresponding NMIs: Germany (PTB), United Kingdom (NPL), France (LNE), Finland (MIKES), Switzerland (METAS), Korea (KRISS), and Turkey (TÜBITAK). The calibrations were performed at the start and end locations, respectively, with a 14-bit CCC (DE) or a 12-bit CCC (all other locations).

ULCA	Travel	Conveyance	Date	Time btw. cal. (weeks)	T_{min} (°C)	T_{max} (°C)	$\Delta G_I/G_I$ (μA/A)	$\Delta R_{IV}/R_{IV}$ ($\mu\Omega/\Omega$)	$\Delta A_{TR}/A_{TR}$ ($\mu\Omega/\Omega$)
U0006	DE/UK/DE	Air cargo	02/2015	2	8	25	−0.036	−0.404	−0.44
U0007							−0.202	−0.581	−0.783
U0006	DE/FR/DE	Car	03−04/2015	5	18	26	0.158	−0.04	0.118
U0007							−0.142	−0.057	−0.199
U0006	DE/FI	Car	11/2015	3	16	28	0.124	−0.079	0.045
U0007							−0.069	−0.026	−0.094
U0006	FI/DE	Air cargo	05/2016	6	18	23	0.168	−0.056	0.112
U0007							−0.284	−0.075	−0.359
U0006	DE/CH	Car	11/2016	6	8	21	−0.019	−0.1606	−0.1796
U0007				3			0.21	−0.169	0.041
U0006	CH/DE	Air cargo	11/2016	5	7	21	0.301	−0.1324	0.1686
U0007							0.042	−0.235	−0.193
U0006	DE/KR	Air cargo	01/2017	12	−4	25	0.27	−0.609	−0.339
U0007							−0.074	−1.697	−1.771
U0006	KR/DE	Air cargo	05/2017	6	15	25	0.072	−0.062	0.011
U0007							−0.055	−0.051	−0.105
U0010	DE/UK/DE	Air cargo	12/2016−06/2017	29	12	23	0.308	−0.47	−0.162
U0010	DE/UK/DE	Air cargo	08−09/2017	4	16	28	0.201	−0.186	0.015
U0010	DE/TR/DE	Air cargo	09/2017−05/2018	37	10	30	0.561	−0.24	0.321

resulting annual drift for A_{TR} is found between 0.5 $\mu\Omega/\Omega$ and −2 $\mu\Omega/\Omega$ (gray meshed area).

The new noise-optimized variants U0020 and U0033 were monitored since the late 2017. In this interval, they show a remarkably stable behavior both for G_I and R_{IV}.

Instruments U0006, U0007, and U00010 have been sent to different NMIs worldwide to perform measurements or to realize international comparisons (see Table I). In total, there were eight round trips between PTB and other NMIs. This enables a stability investigation under travel. The ULCAs were transported in a hard-protective case by air cargo or by car. During the transport, the temperature was recorded in order to get the minimum and maximum temperatures T_{min} and T_{max}. Note that U0006 and U0007 are two ULCA channels sharing the same housing, i.e. they always experienced the same environmental conditions. Each ULCA was calibrated at the start and end locations, respectively. PTB's 14-bit CCC was used for calibrations in Germany (DE), the 12-bit CCC version[20] in Switzerland (CH) and in Finland (FI). For the calibrations performed in Korea (KR), a commercial version[22] of the 12-bit CCC was used, with an electronics very similar to the 14-bit CCC system used at PTB. All calibration values are referred to 23 °C by means of the internal temperature sensors of the ULCA units.

Table I provides an overview of the changes in G_I, R_{IV}, and A_{TR} for each traveling ULCA, corresponding to the journeys. The relative changes of $\Delta G_I/G_I$, $\Delta R_{IV}/R_{IV}$, and $\Delta A_{TR}/A_{TR}$ are given by subtracting the calibration value before and after transportation. Note that during the stays of U0010 at NPL (both round trips DE/UK/DE), this ULCA was also calibrated with NPL's high-resistance CCC, showing good agreement between the results obtained with the two different CCC systems. These data are not listed in Table I but are published in Ref. 11.

Table I shows that for each transport G_I and R_{IV} typically change by a few parts in 10^7. The time interval between the calibrations before and after travel varied between 2 and
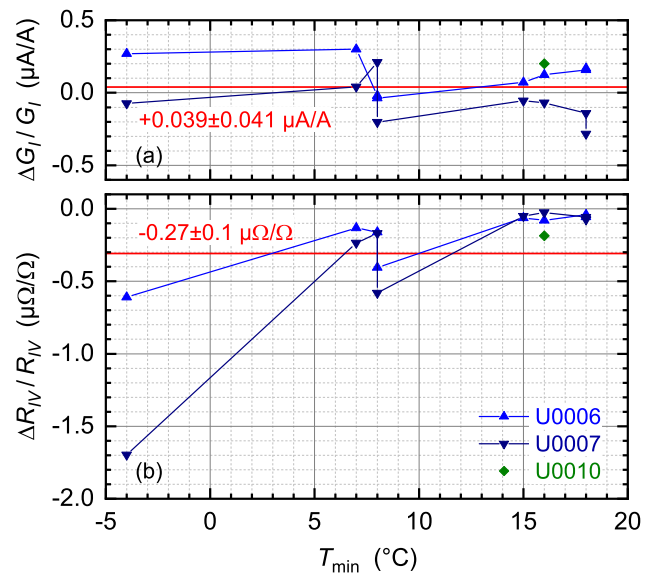

FIG. 5. Influence of T_{min} during transportation: (a) $\Delta G_I/G_I$ and (b) $\Delta R_{IV}/R_{IV}$. Calibration intervals longer than 12 weeks have been omitted to keep the effect of drift low.

37 weeks. For longer periods between calibrations, the drift noticeably contributes to the observed changes. In the case of $\Delta G_I/G_I$ there is no preferential direction of the changes. This behavior is illustrated in Fig. 5(a), which shows the relative changes $\Delta G_I/G_I$ as a function of the lowest recorded temperature T_{min} during transport. In addition, the mean of all data points is indicated by a red line and a corresponding number with uncertainty (standard deviation of the mean). Although strictly speaking the latter is only meaningful when all points are samples of the same distribution, it could indicate a potential trend. The mean change $\Delta G_I/G_I$ of 0.039 μA/A is practically zero for the calculated uncertainty of 0.041 μA/A. In contrast, the changes in R_{IV} caused by travel are always negative. Furthermore, it appears that they are stronger for lower minimum temperatures during travel. The mean of $\Delta R_{IV}/R_{IV}$ in Fig. 5(b) is (-0.29 ± 0.1) $\mu\Omega/\Omega$. Considering the uncertainty, the negative trend is clearly discernible. Note that the ULCA experienced once a very low temperature of –4 °C during a two weeks' delay in customs clearance.

IV. LOW-CURRENT PERFORMANCE

As pointed out in Ref. 16, the accuracy of the CCC is not sufficient to perform stability investigations at sub-nanoampere currents due to the nonlinearity of the SQUID and low-frequency excess noise. At present, there are no current sources available that provide sufficient accuracy in this range. Therefore, we use the advantageous feature of the ULCA to alternatively act as a current source. By using an ULCA pair, a test current can be generated by one unit and simultaneously measured by the other one.[12] Naturally, however, such a setup only yields the combined uncertainty of the ULCA pair, which is a factor of $\sqrt{2}$ larger than that of the individual ULCA in the case of two identical units with uncorrelated fluctuations in A_{TR}. The general measurement setup is schematically shown in Fig. 6. The red colored ULCA represents the current source. Its input stage is configured in the SRC mode and the output stage in the VOUT mode. A voltage V_S applied to the TEST connector generates a source current $I_S = V_S/R$ (with R = 6.75 GΩ for the noise-optimized variant) at the IN connector and at the same time a proportional voltage $V_{OUT,NS}$ at VOUT. The addition "NS" in the subscript indicates that this ULCA is operated in the normal mode (N) as a current source (S). Note that the source voltage V_S at the TEST input is filtered by a low-pass filter. Furthermore, for very low currents, it might be advantageous to generate the required low voltage levels by applying an optional voltage divider.

The blue colored ULCA represents the current meter (amplifier). Its input stage is in the AMP mode and the output stage in the VOUT mode. The source current I_S flows into the input IN, leading to a corresponding voltage $V_{OUT,NA}$ at the output VOUT (subscript "NA" indicates the normal amplifier mode). Ideally, the current $I_{S,NA} = V_{OUT,NA}/A_{TR,NA}$ displayed by the amplifier ULCA is exactly equal to the current $I_{S,NS} = -V_{OUT,NS}/A_{TR,NS}$ monitored by the source ULCA, i.e., $I_{S,NA} = I_{S,NS} = I_S$. Deviations in the ULCA calibration values and the
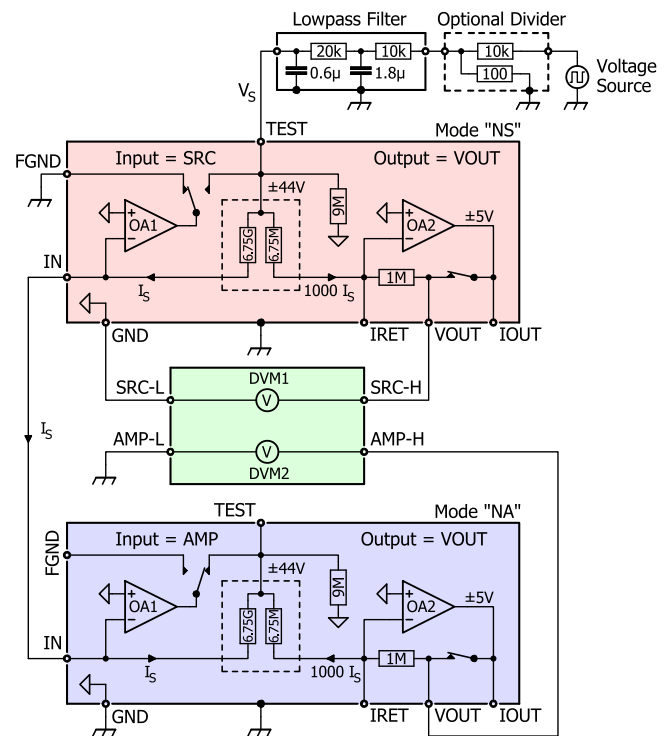

FIG. 6. Setup for the relative stability measurement without CCC. The ULCA colored in red acts as a current source and the one colored blue as a current amplifier. Voltages corresponding to the generated and measured current are measured with two DVMs (green area). The case potentials of the ULCAs are electrically connected.

measurement setup are described here by an error current

$$\Delta I = I_{S,NA} - I_{S,NS} = \frac{V_{OUT,NA}}{A_{TR,NA}} + \frac{V_{OUT,NS}}{A_{TR,NS}} \ . \tag{1}$$

The normalized error current $\Delta I/I_S$ is a measure of the consistency between the experimental difference in the transresistances of the two ULCAs and the difference expected from calibration.

A straightforward method to determine the error current is to measure each ULCA output with a separate digital voltmeter (DVM) as indicated in the green colored box in Fig. 6. DVM1 measures the voltage $V_{OUT,NS}$ between VOUT and GND of the current-generating ULCA via the SRC-H and SRC-L terminals. Through terminals AMP-H and AMP-L, DVM2 measures the voltage $V_{OUT,NA}$ between VOUT and case of the amplifier ULCA. In this scheme, the uncertainties of the DVMs directly affect the result. Therefore, alternative methods have been developed to substantially relax the demands on the voltmeter accuracy. Figure 7 summarizes four basic concepts for the determination of the error current $\Delta I/I_S$. All methods were experimentally tested and found to work well. For the sake of completeness, the already mentioned use of two DVMs is depicted in (a).
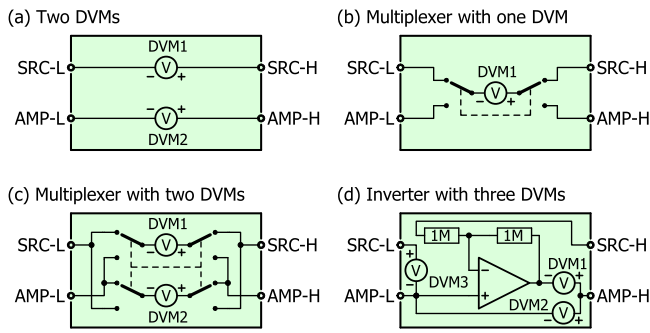
FIG. 7. Four different methods for determining the error current ΔI. The circuit elements enclosed by a frame are substitutes for the two DVMs in Fig. 6. The inverter used in (d) is detailed in Fig. 8.

The method in Fig. 7(b) involves only one DVM and a multiplexer which alternately switches the DVM between the two ULCAs. First results are reported in Ref. 12. As both signals $V_{OUT,NA}$ and $V_{OUT,NS}$ are measured with the same DVM and are nominally equal in amplitude, the uncertainty contributions of the DVM gain and linearity are suppressed. Unfortunately, the sequential measurement increases the measurement time by a factor of two because each signal is measured only half of the time. In practice, the increase in measurement time is even higher due to low-frequency fluctuations from the voltage sources. The measurement time can be minimized by increasing the switching rate up to about 0.1 Hz, limited by transient effects after current reversal.

Figure 7(c) represents an approach using two DVMs in combination with a multiplexer. This allows a reduction in measurement time because both signals are measured simultaneously throughout the measurement: DVM1 measures $V_{OUT,NS}$ while DVM2 measures $V_{OUT,NA}$ and vice versa. The effect of low-frequency fluctuations in the voltage source is also strongly suppressed. Still, the stability of the DVMs affects the uncertainty.

All methods mentioned so far determine the small error signal ΔI by measuring both output signals individually. An even better approach is based on measuring the small error signal of interest directly, rather than by deriving it from the difference of relatively large quantities of similar amplitude. Due to the opposite polarity of the source and amplifier output, the difference signal is not directly available. Hence, in Fig. 7(d) the sign of $V_{OUT,NS}$ is reversed by using an extra inverter circuit. As a result, the error signal can now be directly measured, and the demands on the DVM accuracy are strongly relaxed. Effectively, this inverter method shifts the accuracy demands from the DVMs to the inverter.

A sufficiently accurate inverter can be built by using two calibrated ULCA output stages (see Fig. 8). The inverter consists of two equal resistors (here 1 MΩ) and an operational amplifier. The bottom ULCA in Fig. 8 provides the operational amplifier with feedback resistor, while the upper one is used
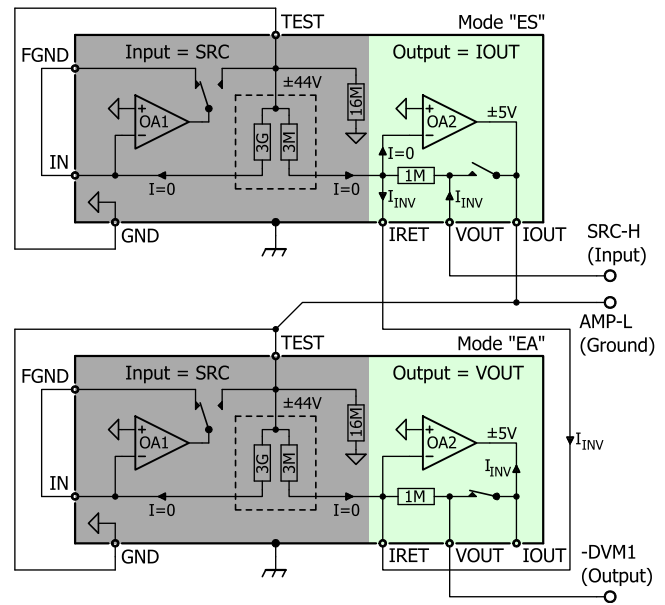

FIG. 8. Setup for using two ULCA output stages as a highly accurate inverter as required in Fig. 7(d). In the upper ULCA, R_{IV} = 1 MΩ is used as passive resistor. In the lower ULCA, OA2 and R_{IV} = 1 MΩ serve as amplifier and feedback resistor, respectively. The inverter input is SRC-H, the ground potential is AMP-L, and the output is -DVM1 (negative input of DVM1) corresponding to the labeling in Fig. 7. The ULCA case potentials are connected to each other.

as a passive resistor. This resistor is disconnected from the output of the corresponding amplifier OA2. The output IOUT is connected to the inverter ground (AMP-L) to form a servo loop that keeps the current output terminal IRET at internal ground potential. This provides proper operation of OA2 and ensures that the current flowing into the amplifier input is practically zero due to the high open-loop gain. The input stages of the two ULCAs (gray areas in Fig. 8) are configured such that they do not disturb the inverter function.

Three DVMs are utilized for the inverter-based configuration in Fig. 7(d). DVM1 measures the voltage difference V_1 between AMP-H (output of the amplifier ULCA) and the inverted output of the source ULCA. DVM2 meters the voltage V_2 between AMP-H and AMP-L, i.e., the output voltage $V_{OUT,NA}$ that is referred to the central measurement ground (case potential). DVM3 senses the voltage V_3 between SRC-L and AMP-L, i.e., the internal ground potential of the source ULCA to which the output $V_{OUT,NS}$ is referred to. The output voltage of the inverter against measurement ground AMP-L amounts to

$$V_{OUT,EA} = V_2 - V_1 = \frac{R_{IV,EA}}{R_{IV,ES}}(I_{S,NS} A_{TR,NS} - V_3), \qquad (2)$$

where the subscripts "ES" and "EA" indicate extended source and extended amplifier mode, respectively.[19] By transposing Eq. (1) for $I_{S,NS}$, inserting it into Eq. (2), and rearranging the

result, one obtains the reduced error current

$$\frac{\Delta I}{I_{S,NA}} = 1 - \frac{A_{TR,NA}}{A_{TR,NS}}\left[\frac{R_{IV,ES}}{R_{IV,EA}}\left(1-\frac{V_1}{V_2}\right)+\frac{V_3}{V_2}\right]. \quad (3)$$

Equation (3) shows that the demands on the accuracy and linearity of the DVMs are low because V_1/V_2 and V_3/V_2 represent small relative deviations $\ll 1$. The common-mode rejection (CMR) of DVM1, however, needs to be very high because both input terminals are at high potential. In the datasheet of the 3458A multimeter employed, a CMR of >90 dB is specified for a 1 kΩ imbalance in the LO lead.[23] To determine the CMR without imbalance, we applied a square wave to both inputs HI and LO of a 3458A multimeter and measured the displayed peak-peak amplitude. A cycle duration of 100 s and peak-peak values of up to 10 V were selected. No signal was detectable within the uncertainty of 4 nV. For the ULCA measurement at ±100 pA (200 mV common-mode signal) this corresponds to a uncertainty contribution of 2 parts in 10^8.

The method with inverter according to Fig. 7(d) was utilized to evaluate the accuracy of the noise-optimized ULCA. Figure 9 shows the measured relative error current $\Delta I/I_S \approx \Delta I/I_{S,NA}$ of units U0020 and U0033. Here, U0033 was used as the current source and U0020 was the current meter (amplifier). The inverter was built up with two standard ULCAs. Before the measurement all ULCA stages were calibrated with the 14-bit CCC. The calibration results were used to determine the error current according to Eq. (3) from the measured DVM readings. For the evaluation, 5 mΩ was added to the transresistance $R_{IV,ES}$ to account for a small parasitic resistance due

to the wiring. The time axis in Fig. 9 is referred to the calibration date of the noise-optimized ULCA input stages, which are calibrated with an uncertainty of 20 parts in 10^9 (see Ref. 18). All other ULCA stages have a lower calibration uncertainty of 10 parts in 10^9. The calibration of the total transresistance A_{TR} of the noise-optimized ULCA has a combined uncertainty of $\sqrt{20^2+10^2} \approx 22$ parts in 10^9. For the total calibration uncertainty of the six ULCA stages, we estimate $\sqrt{2\times20^2+4\times10^2} \approx 35$ parts in 10^9, indicated by the green hatched area in Fig. 9.

The CCC calibration uses a 20 s cycle with current reversal every 10 s. The first 5 s after each current reversal is disregarded. This removes the settling effects but increases the statistical uncertainty at any given measurement time. Therefore, for the low current measurement with the inverter circuit, the cycle time was increased to 100 s (90% data usage instead of 50%). Although the system noise increases slightly from 2.3 fA/$\sqrt{Hz}$ to 2.7 fA/$\sqrt{Hz}$ due to the longer cycle time, the overall statistical uncertainty was reduced. To make sure that the cycle time has no effect on the result, high current measurements were performed for both cycle times. The agreement between both results was well within the uncertainty. The current was limited by the voltage source to ±1.45 nA compared to ±6.1 nA for the CCC calibration. For the low-current experiments we selected ±100 pA, a typical value for SEPs.[1,2,9,24] The integration time was one day and the total measurement duration was 10 days. The mean value over this period was (-60 ± 15) nA/A (red line in Fig. 9). This result does not overlap with the CCC calibration within the standard uncertainty, but is consistent within the expanded uncertainty at $k = 2$ (95% confidence level). The measurements show that the accuracy and linearity of the noise-optimized ULCA is below one part in 10^7 down to the low current levels relevant for SEP research. One might argue that the current dependence (nonlinearity) of the ULCA inverter leads to a
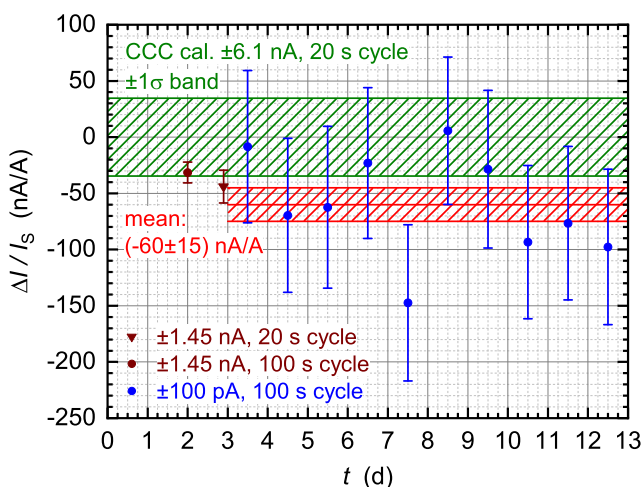

FIG. 9. Relative error current $\Delta I/I_S$ of two noise-optimized ULCA units U0020 and U0033 configured for a measurement setup according to Fig. 6. The inverter mode in Figs. 7(d) and 8 was applied. The green hatched area shows the standard uncertainty of the CCC calibration. The quoted cycle durations of 20 s or 100 s indicate that the current was reversed every 10 s or 50 s, respectively. The first 5 s after each current reversal were disregarded to suppress settling effects. At a high current of ±1.45 nA the integration time was about 4 h or 6 h, while at ±100 pA it was increased to one day.
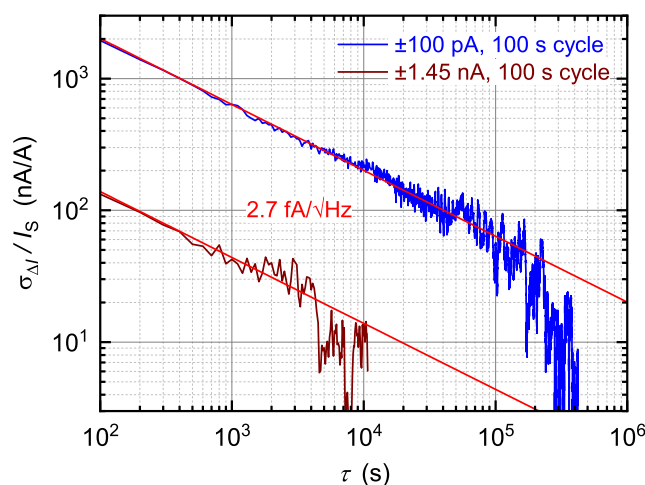

FIG. 10. Allan deviation of the 100 s cycle measurements in Fig. 9. The red lines correspond to a white noise floor of 2.7 fA/$\sqrt{Hz}$ for both current levels.

deviation. However, considering the low power in the resistors of the output stage (18 nW per VHP101[21] during calibration) and the high open-loop gain of the output amplifier ($>10^9$)[10] it is unlikely that there is a significant change between calibration and operation.

In Fig. 10 the corresponding Allan deviation plots of both measurements with 100 s cycle time are plotted. The white noise floor is 2.7 fA/$\sqrt{\text{Hz}}$, dominated by the contribution of the two noise-optimized ULCAs ($\sqrt{2} \times 1.6$ fA/$\sqrt{\text{Hz}} \approx 2.3$ fA/$\sqrt{\text{Hz}}$). The slight increase in noise is not observed for short cycle times and therefore presumably caused by low frequency excess noise. The noise is white in the full range depicted in Fig. 10. An uncertainty of one part in 10^7 is obtained in less than a day, and the stability of the ULCAs is well below one part in 10^7 over the complete period of 10 days.

V. CONCLUSION

A noise-optimized ULCA was compared to the standard variant. Long-term tests with CCC have shown a remarkable stability since the start of the recordings in mid-2014. Typically, the annual drift in A_{TR} of the standard variant remains within $+0.5 \mu\Omega/\Omega$ and $-2 \mu\Omega/\Omega$. A transfer stability of a few parts in 10^7 is achieved if the ULCA is not exposed to extreme temperatures during transport. The new noise-optimized ULCA exhibits the same stability level over the first nine months of observation. Due to the reduced noise level of 1.6 fA/$\sqrt{\text{Hz}}$, the noise-optimized variant reduces the measurement time by up to a factor of two.

By using a special setup with an ULCA inverter, it was demonstrated that the stability and accuracy evaluated by CCC calibration at high current holds down to low current levels of ±100 pA. Uncertainties of well below one part in 10^7 were achieved over a period of 10 days without recalibration. In combination with the reduced noise level, the new ULCA variant (commercialization is planned for 2019)[7] is ideally suited for research on SEPs and other low current devices. For substantially lower uncertainties approaching the calibration uncertainty of about 22 parts in 10^9 (which in absolute terms equals an uncertainty of only 14 elementary charges e per second at a current of 100 pA), frequent calibration with the 14-bit CCC is required and extreme care is essential to avoid systematic errors in the measurement setup.

ACKNOWLEDGMENTS

REFERENCES

[1] N.-H. Kaneko, S. Nakamura, and Y. Okazaki, "A review of the quantum current standard," Meas. Sci. Technol. **27**, 032001 (2016).

[2] J. P. Pekola, O.-P. Saira, V. F. Maisi, A. Kemppinen, M. Möttönen, Y. A. Pashkin, and D. V. Averin, "Single-electron current sources: Toward a refined definition of the ampere," Rev. Mod. Phys. **85**, 1421–1472 (2013).

[3] H. Scherer and H. W. Schumacher, "Single-electron pumps and quantum current metrology in the revised SI," Ann. Phys. (submitted).

[4] S. Giblin, M. Kataoka, J. Fletcher, P. See, T. Janssen, J. Griffiths, G. Jones, I. Farrer, and D. Ritchie, "Towards a quantum representation of the ampere using single electron pumps," Nat. Commun. **3**, 930 (2012).

[5] G.-D. Willenberg, "EUROMET.EM-S24: Supplementary comparison of small current sources," Metrologia **50**, 01002 (2013).

[6] D. Drung, C. Krause, U. Becker, H. Scherer, and F. J. Ahlers, "Ultrastable low-noise current amplifier: A novel device for measuring small electric currents with high accuracy," Rev. Sci. Instrum. **86**, 024703 (2015).

[7] Magnicon, ULCA-1, 2016.

[8] H. Scherer and B. Camarota, "Quantum metrology triangle experiments: A status review," Meas. Sci. Technol. **23**, 124010 (2012).

[9] F. Stein, H. Scherer, T. Gerster, R. Behr, M. Götz, E. Pesel, C. Leicht, N. Ubbelohde, T. Weimann, K. Pierz, H. W. Schumacher, and F. Hohls, "Robustness of single-electron pumps at sub-ppm current accuracy level," Metrologia **54**, S1–S8 (2016).

[10] D. Drung, C. Krause, S. P. Giblin, S. Djordjevic, F. Piquemal, O. Séron, F. Rengnez, M. Götz, E. Pesel, and H. Scherer, "Validation of the ultrastable low-noise current amplifier as travelling standard for small direct currents," Metrologia **52**, 756–763 (2015).

[11] S. P. Giblin, D. Drung, M. Götz, and H. Scherer, "Inter-laboratory nanoamp current comparison with sub-part-per-million uncertainty," IEEE Trans. Instrum. Meas. (to be published).

[12] H. Scherer, D. Drung, C. Krause, and M. Götz, "Electrometer calibration with sub-part-per-million uncertainty," IEEE Trans. Instrum. Meas. (to be published).

[13] C. Krause, D. Drung, and H. Scherer, "Measurement of sub-picoampere direct currents with uncertainties below ten attoamperes," Rev. Sci. Instrum. **88**, 024711 (2017).

[14] P. Horowitz and W. Hill, *The Art of Electronics* (Cambridge University Press, 2015).

[15] M. Götz, E. Pesel, and D. Drung, "A compact 14-bit cryogenic current comparator," in *29th Conference on Precision Electromagnetic Measurements (CPEM 2014)* (IEEE, 2014).

[16] D. Drung, M. Götz, E. Pesel, and H. Scherer, "Improving the traceable measurement and generation of small direct currents," IEEE Trans. Instrum. Meas. **64**, 3021–3030 (2015).

[17] S. P. Giblin, M.-H. Bae, N. Kim, Y.-H. Ahn, and M. Kataoka, "Robust operation of a GaAs tunable barrier electron pump," Metrologia **54**, 299–306 (2017).

[18] M. Götz, D. Drung, C. Krause, U. Becker, and H. Scherer, "Calibrating ultrastable low-noise current amplifiers of the second generation with a cryogenic current comparator," IEEE Trans. Instrum. Meas. (published online).

[19] D. Drung and C. Krause, "Ultrastable low-noise current amplifiers with extended range and improved accuracy," IEEE Trans. Instrum. Meas. **66**, 1425–1432 (2016).

[20] M. Götz, D. Drung, E. Pesel, H.-J. Barthelmess, C. Hinnrichs, C. Assmann, M. Peters, H. Scherer, B. Schumacher, and T. Schurig, "Improved cryogenic current comparator setup with digital current sources," IEEE Trans. Instrum. Meas. **58**, 1176–1182 (2009).

[21] Vishay Precision Group, "Ultra-high precision hermetically sealed bulk metal® foil resistor with zero TCR, no humidity effect and 0.005% tolerance within a unique construction, minimizing the effects of stress factors" (2010) http://www.vishaypg.com/docs/63003/vhp100.pdf.

[22] Magnicon, CCC System, 2013 http://www.magnicon.com/metrology/ccc-system/.

[23] Keysight, Keysight 3458A Datasheet, 2010 http://literature.cdn.keysight.com/litweb/pdf/5965-4971E.pdf.

[24] F. Stein, D. Drung, L. Fricke, H. Scherer, F. Hohls, C. Leicht, M. Götz, C. Krause, R. Behr, E. Pesel, K. Pierz, U. Siegner, F. J. Ahlers, and H. W. Schumacher, "Validation of a quantized-current source with 0.2 ppm uncertainty," Appl. Phys. Lett. **107**, 103501 (2015).